Biogeosciences, 12, 1447–1458, 2015
www.biogeosciences.net/12/1447/2015/
doi:10.5194/bg-12-1447-2015

Biogeosciences Open Access

Seasonal response of air–water CO_2 exchange along the land–ocean aquatic continuum of the northeast North American coast.

G. G. Laruelle[1,2], R. Lauerwald[1,3], J. Rotschi[1,4], P. A. Raymond[5], J. Hartmann[6], and P. Regnier[1]

[1]Department of Earth and Environmental Sciences, CP 160/02, Université Libre de Bruxelles, 1050 Brussels, Belgium
[2]Department of Earth Sciences – Geochemistry, Faculty of Geosciences, Utrecht University, 3508 TA Utrecht, the Netherlands
[3]Institut Pierre-Simon Laplace, CNRS – FR636, 78280 Guyancourt CEDEX, France
[4]Department of Bioscience – Center for Geomicrobiology, Aarhus University, 8000 Aarhus, Denmark
[5]Yale School of Forestry and Environmental Studies, New Haven, Connecticut 06511, USA
[6]Institute for Geology, KlimaCampus, Universität Hamburg, Bundesstrasse 55, 20146 Hamburg, Germany

Correspondence to: G. G. Laruelle (goulven.gildas.laruelle@ulb.ac.be)

Received: 17 June 2014 – Published in Biogeosciences Discuss.: 6 August 2014
Revised: 14 November 2014 – Accepted: 27 January 2015 – Published: 5 March 2015

Abstract. This regional study quantifies the CO_2 exchange at the air–water interface along the land–ocean aquatic continuum (LOAC) of the northeast North American coast, from streams to the shelf break. Our analysis explicitly accounts for spatial and seasonal variability in the CO_2 fluxes. The yearly integrated budget reveals the gradual change in the intensity of the CO_2 exchange at the air–water interface, from a strong source towards the atmosphere in streams and rivers ($3.0 \pm 0.5\,\mathrm{TgC\,yr^{-1}}$) and estuaries ($0.8 \pm 0.5\,\mathrm{TgC\,yr^{-1}}$) to a net sink in continental shelf waters ($-1.7 \pm 0.3\,\mathrm{TgC\,yr^{-1}}$). Significant differences in flux intensity and their seasonal response to climate variations is observed between the North and South sections of the study area, both in rivers and coastal waters. Ice cover, snowmelt, and intensity of the carbon removal efficiency through the estuarine filter are identified as important control factors of the observed spatiotemporal variability in CO_2 exchange along the LOAC.

1 Introduction

Over the past decade, several syntheses have highlighted the significant contribution of the land–ocean aquatic continuum (LOAC) to the global atmospheric CO_2 budget (Cole et al., 2007; Battin et al., 2009; Mackenzie et al., 2012; Bauer et al., 2013; Ciais et al., 2013; Raymond et al., 2013; Regnier et al., 2013a). In a recent review, Regnier et al. (2013a) proposed that inland waters (streams, rivers and lakes) and estuaries outgas 1.1 and $0.25\,\mathrm{PgC\,yr^{-1}}$, respectively, while continental shelf seas take up $0.2\,\mathrm{PgC\,yr^{-1}}$. However, CO_2 data are too sparse and unevenly distributed to provide global coverage and large uncertainties remain associated with these estimates. The inland water outgassing could for instance reach $2.1\,\mathrm{PgC\,yr^{-1}}$ with 86 % coming from streams and rivers (Raymond et al., 2013), a value which is about twice that reported in Regnier et al. (2013a) and in the IPCC Fifth Assessment Report (Ciais et al., 2013). The most recent global budgets for the estuarine CO_2 source and the continental shelf CO_2 sink also reveal significant discrepancies, both falling within the $0.15–0.4\,\mathrm{PgC\,yr^{-1}}$ range (Laruelle et al., 2010, 2013; Cai, 2011; Bauer et al., 2013; Dai et al., 2013). None of these estimates, however, fully resolves the seasonality in CO_2 fluxes because temporal coverage of the global data is insufficient. Complex seasonal dynamics of CO_2 exchanges between the atmosphere and individual components of the LOAC have been reported in previous studies which have highlighted the potential importance of the intra-annual variability for local and regional CO_2 budgets (e.g., Kempe, 1982; Frankignoulle et al., 1998; Jones and Mulholland, 1998; Degrandpré et al., 2002; Thomas and Schneider, 1999; Wallin et al., 2011; Regnier et al., 2013a; Rawlins et al., 2014). Here, we extend the analysis to the sub-continental scale, and present the spatial and seasonal variability of CO_2 fluxes at the air–water interface (FCO_2) for the entire northeast North American LOAC, from streams to the shelf break. This region of unprecedented data coverage allows us to pro-

duce, for the first time, empirically derived monthly maps of CO_2 exchange at 0.25° resolution. Our results allow us to investigate the seasonal CO_2 dynamics across the interconnected systems of the LOAC and elucidating their response to contrasting intra-annual changes in climate conditions.

2 Methods

Our study area is located along the Atlantic coast of the northern US and southern Canada and extends from the Albemarle Sound in the South section to the eastern tip of Nova Scotia in the North section. It corresponds to COSCAT 827 (for Coastal Segmentation and related CATchments) in the global coastal segmentation defined for continental land masses by Meybeck et al. (2006) and extrapolated to continental shelf waters by Laruelle et al. (2013). COSCATs are homogenous geographical units that divide the global coastline into homogeneous segments according to lithological, morphological, climatic, and hydrological properties. The area corresponding to COSCAT 827 comprises 447×10^3 km^2 of watersheds and 357×10^3 km^2 of coastal waters, amongst which 15×10^3 km^2 of estuaries. It is one of the best monitored regions in the world with several regularly surveyed rivers (Hudson, Susquehanna, York, Connecticut) and some of the most extensively studied coastal waters (Degrandpré et al., 2002; Chavez et al., 2007; Fennel et al., 2008; Fennel and Wilkin, 2009; Previdi et al., 2009; Fennel, 2010; Shadwick et al., 2010, 2011; Signorini et al., 2013). For the purpose of this study, the area was divided into a North and a South section (Fig. 1). The boundary is set on land to distinguish the regions subject to seasonal ice freeze and snowfalls from those that are not (Armstrong and Brodzik, 2001). This delineation attributes 96 % of the estuarine surface area to the South section due, for the most part, to the contribution of Chesapeake Bay which accounts for about two thirds of the estuarine area. The delineation extends further into the coastal waters in such a way that the Scotian Shelf and the Gulf of Maine correspond to the North section and the Mid-Atlantic Bight and Georges Bank to the South section. The riverine data are calculated from pH and alkalinity measurements extracted from the GLObal RIver CHemistry Database (GLORICH (Hartmann et al., 2014), previously used in Lauerwald et al., 2013), while continental shelf values are calculated from the Surface Ocean CO_2 Atlas (SOCAT v2.0) database which contains quality controlled direct pCO_2 measurements (http://www.socat.info/, Bakker et al., 2014).

2.1 Rivers

CO_2 evasion from rivers (FCO_2) was calculated monthly per 15 s grid cell (resolution of the hydrological routing scheme HydroSHEDS 15 s, Lehner et al., 2008) from estimates of the effective stream/river surface area A_{eff} [m^2], gas exchange velocity k [m d^{-1}], and water–atmosphere CO_2 concentration gradient $\Delta[CO_2]$ [µmol l^{-1}]:

$$FCO_2 = A_{\text{eff}} \times k \times \Delta[CO_2]. \quad (1)$$

The calculation of A_{eff} first requires estimation of the total stream/river surface area, A. The latter was calculated from the linear stream network derived from the HydroSHEDS 15 s routing scheme using a minimum threshold on the catchment area of 10 km^2, and estimates of stream width derived from the annual mean discharge Q_{ann} using the equations of Raymond et al. (2012, 2013) (Eqs. 2, 3). Values of A were not calculated for each individual month, as the discharge–stream width relationship only hold true for Q_{ann} (Raymond et al., 2013). Q_{ann} was obtained using HydroSHEDS 15 s to route the gridded data of average annual runoff from the UNH/GRDC composites (Fekete et al., 2002).

$$\ln(B[\text{m}]) = 2.56 + 0.423 \times \ln(Q_{\text{ann}}[\text{m}^3\,\text{s}^{-1}])$$

(Eq. 2 after Raymond et al., 2012),

$$\ln(B[\text{m}]) = 1.86 + 0.51 \times \ln(Q_{\text{ann}}[\text{m}^3\,\text{s}^{-1}]$$

(Eq. 3 after Raymond et al., 2013),

where B is stream width [m] and Q_{ann} is annual average discharge [m^3 s^{-1}].

For each 15 s raster cell covered by lake and reservoir areas as represented in the global lake and wetland database of Lehner and Döll (2004), A was set to 0 km^2. A_{eff} was then derived from A to account for seasonal stream drying and ice cover inhibiting FCO_2. Seasonal stream drying was assumed for each 15 s cell and month when the monthly average discharge Q_{month} is 0 m^3 s^{-1}. Values of Q_{month} were calculated similarly to that of Q_{ann} using the gridded data of average monthly runoff from the UNH/GRDC composites (Fekete et al., 2002). Ice cover was assumed for each 15 s cell and month when the mean air temperature (T_{air}), derived from the WorldClim data set of Hijmans et al. (2005), is below −4.8° C (Lauerwald et al., 2015). In case of ice cover and/or stream drying, A_{eff} is set to 0 m^2. Otherwise A_{eff} equals A.

Values of k were first calculated as standardized values for CO_2 at a water temperature (T_{water}) of 20° C (k_{600}), from stream channel slope CS and estimates of flowing velocity V (Eq. 4). Using the Strahler order (Strahler, 1952) to perform the segmentation of the stream network, CS was calculated for each segment by dividing the change in its altitude by its length. Information on altitude was derived from the HydroSHEDS elevation model. V was calculated from Q_{ann} based on the equations of Raymond et al. (2012, 2013) (Eqs. 5, 6). Similarly to the stream width, the $V - Q$ relationship only holds true for Q_{ann} (Raymond et al., 2013), and this is why only annually average values for V and k_{600} could be

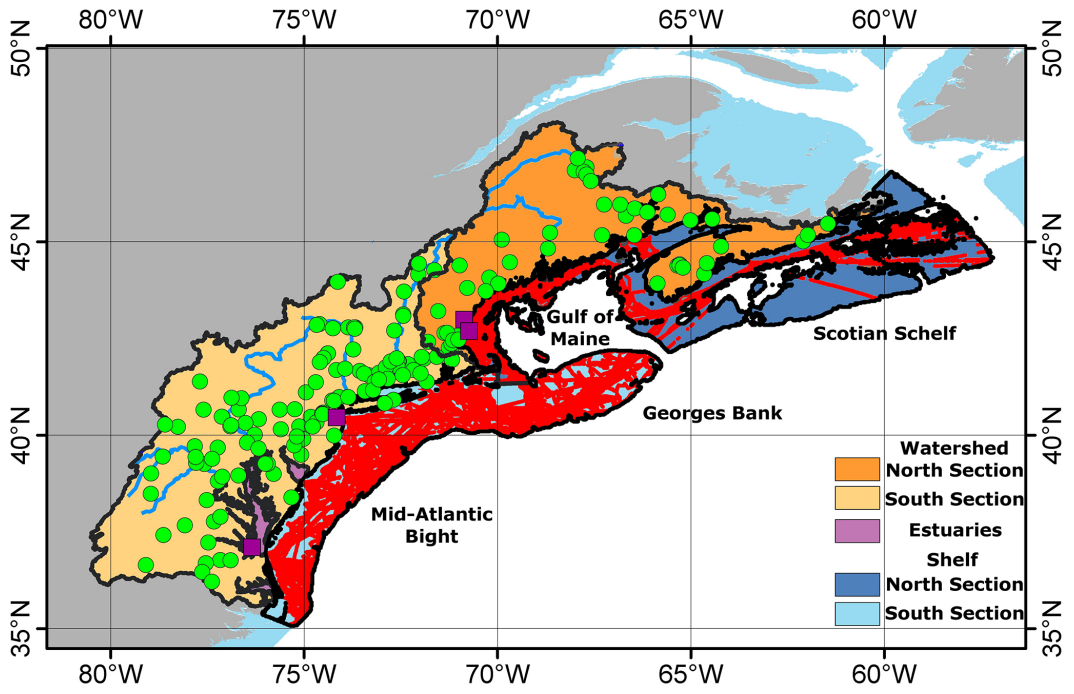

Figure 1. Geographic limits of the study area with the location of the riverine (GLORICH database, in green; Lauerwald et al., 2013) and continental shelf waters data used for our calculations (SOCAT 2.0 database, in red; Bakker et al., 2014). The location of the estuarine studies used is indicated by purple squares.

calculated. The k value for each month was calculated from k_{600}, an estimate of the average monthly water temperature T_{water} (Lauerwald et al., 2015; Raymond et al., 2012).

$$k_{600}[\mathrm{m\,d^{-1}}] = V[\mathrm{m\,s^{-1}}] \times \mathrm{CS}[1] \times 2841 + 2.02$$

(Eq. 4 after Raymond et al., 2012),

$$\ln(V[\mathrm{m\,s^{-1}}]) = -1.64 + 0.285 \times \ln(Q_{\mathrm{ann}}[\mathrm{m^3\,s^{-1}}])$$

(Eq. 5 after Raymond et al., 2012),

$$\ln(V[\mathrm{m\,s^{-1}}]) = -1.06 + 0.12 \times \ln(Q_{\mathrm{ann}}[\mathrm{m^3\,s^{-1}}])$$

(Eq. 6 after Raymond et al., 2013),
where k_{600} is the standardized gas exchange velocity for CO_2 at 20° C water temperature [$\mathrm{m\,d^{-1}}$], Q_{ann} is annual average discharge [$\mathrm{m^3\,s^{-1}}$], V stream flow velocity [$\mathrm{m\,s^{-1}}$], and CS channel slope [dimensionless].

Values of $\Delta(CO_2)$ were derived from monitoring data with calculated $p\mathrm{CO_{2river}}$ (12 300 water samples, from 161 locations, Lauerwald et al., 2013), and an assumed $p\mathrm{CO_{2atmosphere}}$ of 390 µatm. Lauerwald et al. (2013) calculated $p\mathrm{CO_{2river}}$ values from pH, alkalinity, water temperature, and, where available, major ion concentrations, using the hydrochemical modeling software PhreeqC v2 (Parkhurst and Appelo, 1999). The $p\mathrm{CO_2}$ values were converted into concentrations, [CO_2], using Henry's constant (Henry, 1803) for each sample at its observed temperature T_{water} using the equation of Telmer and Veizer (1999). In order to minimize the influence of extreme values, the results were aggregated to median values per sampling location and month for which at least three values were available. These median values per sampling location and month were then used to calculate maps of $\Delta[CO_2]$ at a 15 s resolution. To this end, an inverse distance-weighted interpolation was applied. This method allows us to predict a value for each grid cell from observed values at the four closest sampling locations, using the inverse of the squared distance between the position on the grid and each sampling locations as weighting factors. To account for downstream decreases in $p\mathrm{CO_{2river}}$, which are often reported in the literature (Finlay, 2003; Teodoru et al., 2009; Butman and Raymond, 2011), the interpolation was applied separately to three different classes of streams and rivers defined by Q_{ann}, for which sufficiently large subsets of sampling locations could be retained: (1) $Q_{\mathrm{ann}} < 10\,\mathrm{m^3\,s^{-1}}$ ($n = 76$), (2) $10\,\mathrm{m^3\,s^{-1}} \le Q_{\mathrm{ann}} < 100\,\mathrm{m^3\,s^{-1}}$ ($n = 47$), and (3) $Q_{\mathrm{ann}} \ge 100\,\mathrm{m^3\,s^{-1}}$ ($n = 38$). The three maps of $\Delta[CO_2]$ per month were then recombined according to the spatial distribution of Q_{ann} values. The FCO_2 values were first calculated using Eq. (1) at the high spatial resolution of 15 s for each month. The results were then aggregated to a 0.25° resolution and 3-month period and reported as area-specific values referring to the total surface area of the grid cell. At the outer boundaries, only the proportions of the cell covered by our study area are taken into account. The difference between the

FCO_2 values calculated using the equations of Raymond et al. (2012) and Raymond et al. (2013) was used as an estimate of the uncertainty of the mean yearly FCO_2. The aforementioned method is consistent with the approach of Raymond et al. (2013), which used two distinct sets of equations for k and A to estimate the uncertainty in these parameters and their combined effect on the estimated FCO_2.

2.2 Estuaries

The yearly averaged CO_2 exchange at the air–water interface was obtained from local estimations of emission rates in seven estuaries located within the study area (see Table 1). The limited number of observations does not allow us to resolve the seasonality in CO_2 emissions. The yearly average local CO_2 emission rates range from 1.1 molC m^{-2} yr^{-1} in the Parker River to 9.6 molC m^{-2} yr^{-1} in the Hudson River estuary, for a mean value of 4.2 molC m^{-2} yr^{-1} for the seven systems. This value was then multiplied by the estuarine surface areas extracted from the SRTM water body data set (NASA/NGA, 2003), to estimate the bulk outgassing for the North and South sections of COSCAT 827. It should be noted that the methods used to estimate the CO_2 emission rates differ from one study to the other (i.e., different relationships relating wind speed to the gas transfer coefficient). However, in the absence of a consistent and substantial estuarine pCO_2 database for the region, we believe that our method is the only one which allows one to derive a regional data driven estimate for the CO_2 outgassing from estuaries which would otherwise require the use of reactive transport models (Regnier et al., 2013b). Similar approaches have been used in the past to produce global estuarine CO_2 budgets (Borges et al., 2005; Laruelle et al., 2010, 2013; Cai, 2011; Chen et al., 2013). The standard deviation calculated for the emission rates of all local studies was used as an estimate of the uncertainty of the regional estuarine FCO_2.

2.3 Continental shelf waters

Monthly CO_2 exchange rates at the air–water interface were calculated in continental shelf waters using 274 291 pCO_2 measurements extracted from the SOCAT 2.0 database (Bakker et al., 2014). For each measurement, an instantaneous local CO_2 exchange rate with the atmosphere was calculated using Wanninkhof's equation (Wanninkhof, 1992), which is a function of a transfer coefficient (k), dependent on the square of the wind speed above sea surface, the apparent solubility of CO_2 in water (K_0') [moles m^{-3} atm^{-1}], which depends on surface water temperature and salinity, and the gradient of pCO_2 at the air–water interface (ΔpCO_2) [µatm].

$$FCO_2 = A_s \times k \times K_0' \times \Delta pCO_2 \quad (2)$$

The parameterization used for k is that of Wanninkhof et al. (2013), and all the data necessary for the calculations are available in SOCAT 2.0 except for wind speed, which was extracted from the CCMP database (Atlas et al., 2011). The resulting CO_2 exchange rates were then averaged per month for each 0.25° cell in which data were available. Average monthly CO_2 exchange rates were calculated for the North and South sections using the water surface area and weighted rate for each cell, and those averages were then extrapolated to the entire surface area A_s of the corresponding section to produce FCO_2. In effect, this corresponds to applying the average exchange rate of the section to the cells devoid of data. To refine further the budget, a similar procedure was also applied to 5 depth segments (S1 to S5) corresponding to 0–20, 20–50, 50–80, 80–120 and 120–150 m, respectively, and their respective surfaces areas were extracted from high resolution bathymetric files (Laruelle et al., 2013). The choice of slightly different methodologies for FCO_2 calculations in rivers and continental shelf waters stems from the better data coverage in the continental shelf, which allows the capturing of spatial heterogeneity within the region without using interpolation techniques. The standard deviation calculated for all the grid cells of the integration domain was used as the uncertainty of the yearly estimates of FCO_2. A more detailed description of the methodology applied to continental shelf waters at the global scale is available in Laruelle et al. (2014).

3 Results and discussion

Figure 2 shows the spatial distribution of FCO_2 along the LOAC integrated per season. Throughout the year, river waters are a strong source of CO_2 for the atmosphere. Significant differences in the intensity of the CO_2 exchange at the air–water interface can nevertheless be observed between the North and South sections, both in time and space. During winter, there is nearly no CO_2 evasion from rivers in the North section due to ice coverage and stream drying. Over the same period, the CO_2 emissions from the South section range from 0 to 5 gC m^{-2} $season^{-1}$. During spring, the pattern is reversed and rivers in the North exhibit higher outgassing rates than in the South section with maximum emissions rates of >10 gC m^{-2} $season^{-1}$. This trend is maintained throughout summer while during fall, the entire COSCAT displays similar emission rates without a clear latitudinal signal. Continental shelf waters display a very different spatial and seasonal pattern than that of rivers. During winter, the North section is predominantly a mild CO_2 sink, with rates between $+2$ and -5 gC m^{-2} $season^{-1}$, which intensifies significantly in the South section (-2 to >-10 gC m^{-2} $season^{-1}$). During spring, an opposite trend is observed, with a quasi-neutral CO_2 uptake in the South section and a strong uptake in the North section, especially on the Scotian Shelf. The entire COSCAT becomes a net CO_2 source in summer with emission rates as high as 5 gC m^{-2} $season^{-1}$ in the Mid-Atlantic Bight. During fall, the Gulf of Maine and Georges Bank remain CO_2 sources,

Table 1. Summary of the data used for the FCO_2 calculations in compartment of the LOAC.

Compartment	Parameter	Description	Source	Reference
Rivers	pCO2	CO_2 partial pressure	GLORICH Lauerwald et al. (2013)	Hartmann et al. (2014)
	–	River network, digital elevation model (DEM)	HydroSHEDS 15 s	Lehner et al. (2008)
	–	Runoff	UNH/GRDC	Fekete et al. (2002)
	T	Air temperature	–	Hijmans et al. (2005)
	–	Lake surface area	Global Lake and Wetland Database	Lehner and Döll (2004)
Estuaries	A_S	Surface Area	SRTM water body data set	NASA/NGA (2003)
	–	CO_2 exchange rate	Average of local estimates	Raymond et al. (1997) Raymond et al. (2000) Raymond and Hopkinson (2003) Hunt et al. (2010)
Shelves	A_S	Surface area	COSCAT/MARCATS Segmentation	Laruelle et al. (2013)
	ΔpCO_2	pCO_2 gradient at the air–water interface	SOCAT database	Bakker et al. (2014)
	k	Calculated using wind Speed	CCMP database	Altas et al. (2011)
	K_0'	Solubility, calculated using salinity, water temperature	SOCAT database	Bakker et al. (2014)

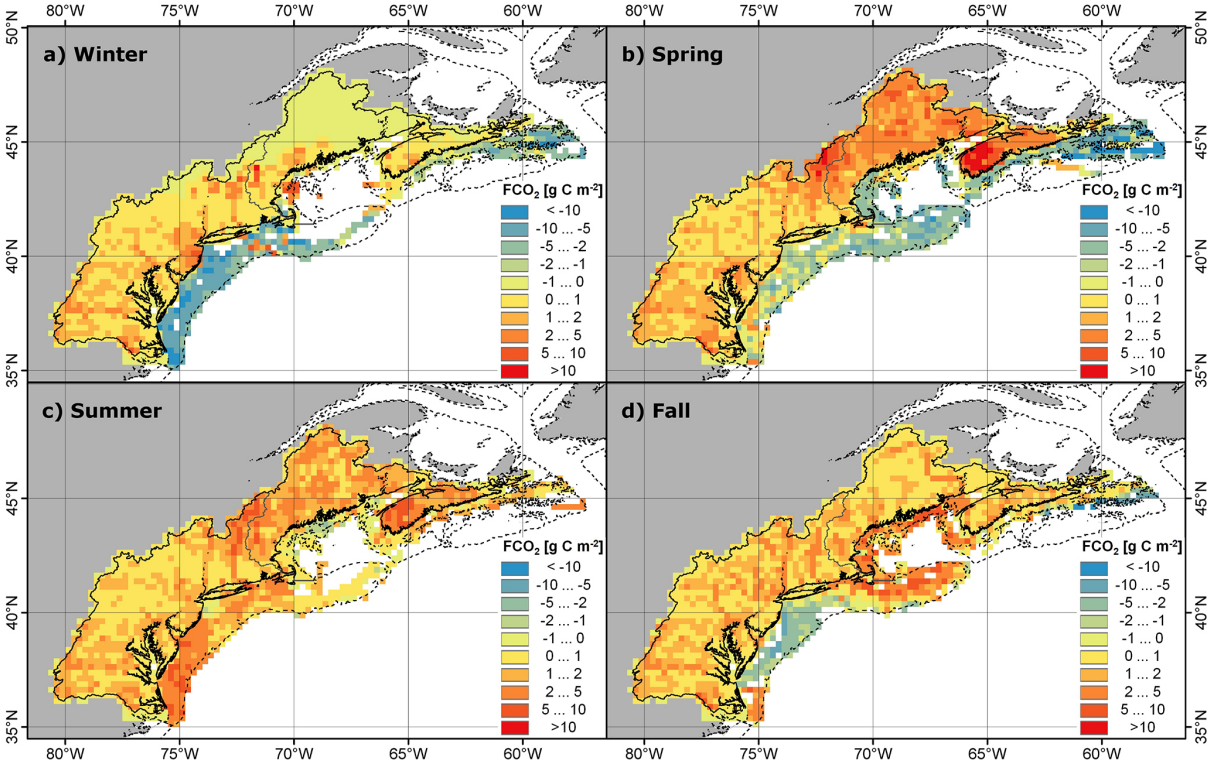

Figure 2. Spatial distribution of the CO_2 exchange with the atmosphere in rivers and continental shelf waters aggregated by seasons. The fluxes are net FCO_2 rates averaged over the surface area of each 0.25° cell and a period of 3 months. Positive values correspond to fluxes towards the atmosphere. Winter is defined as January, February, and March, Spring as April, May, and June, and so forth.

while the Scotian Shelf and the Mid-Atlantic Bight become again regions of net CO_2 uptake.

The monthly integrated fCO_2 for the North and South sections provides further evidence of the contrasting seasonal dynamics for the two areas (Fig. 3a and b). In the North section, CO_2 evasion from rivers is almost zero in January and February, rises to a maximum value of 0.26 ± 0.05 TgC month^{-1} in May and then progressively decreases until the end of the year. These low winter values are explained by the ice cover inhibiting the gas exchange with the atmosphere. The steep increase and fCO_2 maximum in spring could be related to the flushing of water from the thawing top soils, which are rich in dissolved organic carbon (DOC) and CO_2. Additionally, the temperature rise also induces an increase in respiration rates within the water columns(Jones and Mulholland, 1998; Striegl et al., 2012). Rivers and the continental shelf in the North section present synchronized opposite behaviors from winter through spring. In the shelf, a mild carbon uptake takes place in January and February (-0.04 ± 0.25 TgC month^{-1}), followed by a maximum uptake rate in April (-0.50 ± 0.20 TgC month^{-1}). This CO_2 uptake in spring has been attributed to photosynthesis associated with the seasonal phytoplankton bloom (Shadwick et al., 2010). Continental shelf waters behave quasi-neutral during summer ($<0.05 \pm 0.09$ TgC month^{-1}) and emit CO_2 at a high rate in November and December ($>0.15 \pm 0.21$ TgC month^{-1}). Overall, the rivers of the North section emit 1.31 ± 0.24 TgC yr^{-1}, while the continental shelf waters take up 0.47 ± 0.17 TgC yr^{-1}. The very limited estuarine surface area ($0.5\ 10^3$ km^2) only yields an annual outgassing of 0.03 ± 0.02 TgC yr^{-1}. The shelf sink calculated for the region differs from that of Shadwick et al. (2011) which reports a source for the Scotian Shelves, in contrast to the current estimate. Our seasonally resolved budget is however in line with the -0.6 TgC yr^{-1} sink calculated by Signorini et al. (2013) using an 8-year data set as well as with the simulations of Fennel and Wilkin (2009), which also predict sinks of -0.7 and -0.6 TgC yr^{-1} for 2004 and 2005, respectively. No similar analysis was so far performed for inland waters.

In the South section of the COSCAT, the warmer winter temperature leads to the absence of ice cover (Armstrong and Brodzik, 2001). Our calculations predict that the riverine surface area remains stable over time, favoring a relatively constant outgassing between 0.1 and 0.2 TgC month^{-1} throughout the year, adding up to a yearly source of 1.69 ± 0.31 TgC yr^{-1}. Estuaries emit 0.73 ± 0.45 TgC yr^{-1}, because of their comparatively large surface area (14.5×10^3 km^2), about 1 order of magnitude larger than that of rivers (1.2×10^3 km^2, Table 2). It should be noted that our estimate of the estuarine outgassing is derived from a limited number of local studies, none of which were performed in the two largest systems of COSCAT827, which are the Chesapeake and Delaware bays (> 80 % of the total estuarine surface area in COSCAT 827). These estuaries are highly eutrophic (Cai, 2011), which suggests that they might be characterized by lower pCO_2 values and subsequent CO_2 exchange than the other systems in the region. On the other hand, our regional outgassing of 50 gC m^{-2} yr^{-1} is already well below the global average of 218 gC m^{-2} yr^{-1} calculated using the same approach by Laruelle et al. (2013) for tidal estuaries. The continental shelf CO_2 sink is strongest in January (-0.47 ± 0.30 TgC month^{-1}) and decreases until June, when a period of moderate CO_2 emission begins (max of 0.13 ± 0.08 TgC month^{-1} in August) and lasts until October. Finally, November and December are characterized by mild CO_2 sinks. Such seasonal signal, following that of water temperature, is consistent with the hypothesis of a CO_2 exchange in the South section regulated by variations in gas solubility,

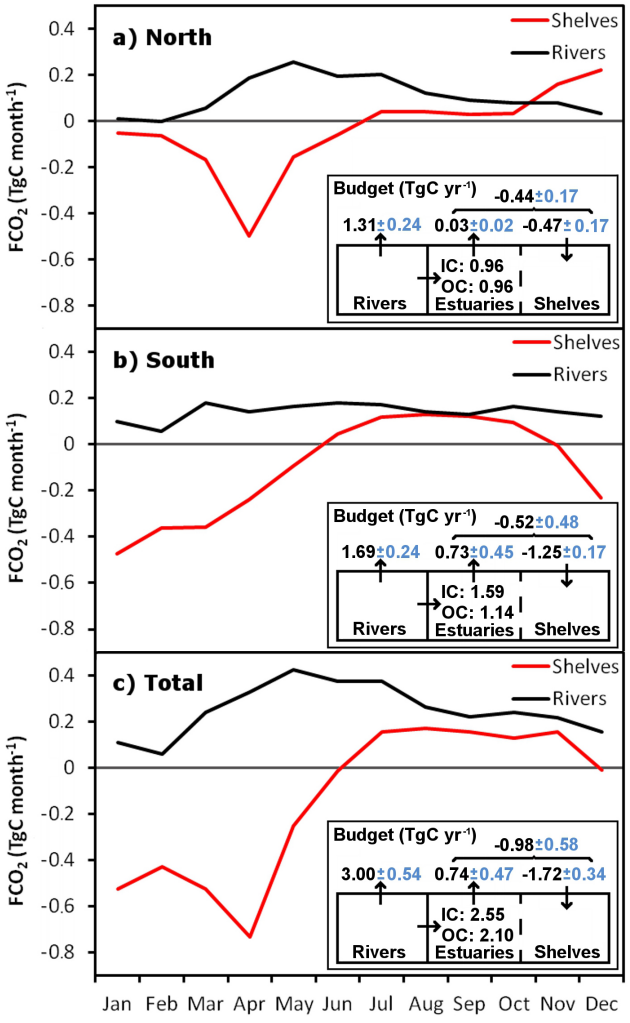

Figure 3. Areal-integrated monthly air–water CO_2 flux for rivers and the continental shelf waters in the North section **(a)**, South section **(b)**, and entire study area **(c)**. Positive values correspond to fluxes towards the atmosphere. The boxes inside each panel correspond to the annual carbon budgets for the region including the lateral carbon fluxes at the river–estuary interface, as inorganic (IC) and organic carbon (OC). The values in grey represent the uncertainties of the annual fluxes.

Table 2. Surface areas, CO_2 exchange rate with the atmosphere, and surface integrated FCO_2 for the North and South sections of COSCAT 827, subdivided by river discharge classes and continental shelf water depth intervals.

	North			South			Total		
	Surface Area 10^3 km^2	Rate gCm^{-2} yr^{-1}	FCO_2 10^9 gC yr^{-1}	Surface Area 10^3 km^2	Rate gCm^{-2} yr^{-1}	FCO_2 10^9 gC yr^{-1}	Surface Area 10^3 km^2	Rate gCm^{-2} yr^{-1}	FCO_2 10^9 gC yr^{-1}
Rivers									
Q1 (Q < 1 m s^{-1})	0.14	2893 ± 521	391 ± 70	0.27	1961 ± 353	532 ± 96	0.41	2271 ± 409	924 ± 166
Q2 (1 m s^{-1} < Q <10 m s^{-1})	0.21	2538 ± 457	525 ± 95	0.32	1570 ± 283	506 ± 91	0.53	1948 ± 351	1032 ± 186
Q3 (10 m s^{-1} < Q <100 m s^{-1})	0.16	1476 ± 267	237 ± 43	0.30	1307 ± 235	392 ± 71	0.46	1366 ± 246	629 ± 113
Q4 (100 m s^{-1} < Q)	0.17	891 ± 160	152 ± 27	0.36	729 ± 131	261 ± 47	0.52	781 ± 141	412 ± 74
Sub-total	0.67	1939 ± 349	1305 ± 235	1.25	1351 ± 243	1692 ± 305	1.92	1557 ± 280	2997 ± 539
Estuaries	0.53	50 ± 31	27 ± 19	14.51	50 ± 31	731 ± 453	15.04	50 ± 31	758 ± 469
Shelf									
S1 (depth <20m)	11.21	5 ± 1	53 ± 19	24.28	−3 ± 1	−79 ± 11	35.49	−1 ± 1	−27 ± 5
S2 (20 m <depth < 50 m)	26.25	−1 ± 1	−35 ± 12	63.88	−8 ± 1	−521 ± 70	90.13	−6 ± 1	−556 ± 108
S3 (50 m <depth < 80 m)	39.28	−3 ± 1	−128 ± 45	48.63	−7 ± 1	−359 ± 126	87.91	−6 ± 1	−488 ± 95
S4 (80 m <depth < 120 m)	60.69	−3 ± 1	−209 ± 73	25.18	−8 ± 1	−199 ± 27	85.87	−5 ± 1	−409 ± 80
S5 (120 m <depth < 150 m)	34.73	−4 ± 1	−151 ± 18	7.63	−12 ± 1	−91 ± 12	42.36	−6 ± 1	−242 ± 47
Sub-total	172.17	−3 ± 1	−472 ± 166	169.59	−7 ± 1	−1250 ± 169	341.77	−5 ± 1	−1722 ± 335

as suggested by Degrandpré et al. (2002) for the Mid-Atlantic Bight.

The analysis of the intensity of the river CO_2 outgassing reveals that the smallest streams (Q < 1 m^3 s^{-1}, Q1 in Table 2) display the highest emission rates per unit surface area, with values ranging from 1961 gC m^{-2} yr^{-1} in the South section to 2893 gC m^{-2} yr^{-1} in the North section. These values gradually decrease with increasing river discharge to 729 gC m^{-2} yr^{-1} in the South section and 891 gC m^{-2} yr^{-1} in the North section for Q > 100 m^3 s^{-1} (Q4, Table 2). The emission rates for this latter class of rivers are consistent with the median emission rate of 720 gC m^{-2} yr^{-1} proposed by Aufdenkampe et al. (2011) for temperate rivers with widths larger than 60–100 m. Aufdenkampe et al. (2011) also report a median emission rate of 2600 gC m^{-2} yr^{-1} for the smaller streams and rivers, which falls on the high end of the range calculated for Q1 in the present study. The surface area of the river network is relatively evenly distributed amongst the four discharge classes of rivers (Table 2). Yet, river sections for which Q < 10 m^3 s^{-1} (Q1+Q2) contribute to 65 % of the total CO_2 outgassing although they only represent 51 % of the surface area. This result therefore highlights that streams and small rivers are characterized by the highest surface-area-specific emission rates. The higher outgassing rates in the North section are a consequence of higher ΔCO_2 values since average k values are similar in both sections. In rivers with Q_{ann}<10 m^3 s^{-1}, the ΔCO_2 is about twice as high in the North than in the South section from April to August (Table 2). The calculation of pCO_2 from alkalinity and pH presumes however that all alkalinity originates from bicarbonate and carbonate ions and thus tends to overestimate pCO_2 because non-carbonate contributions to alkalinity, in particular organic acids, are ignored in this approach. The rivers in Maine and New Brunswick, which drain most of the northern part of COSCAT 827, are characterized by relatively low mineralized, low pH waters, rich in organic matter. In these rivers, the overestimation in pCO_2 calculated from the alkalinity attributed to the carbonate system only was reported to be in the range of 13–66 % (Hunt et al., 2011). Considering that rivers in the southern part of COSCAT 827 have lower DOC concentrations and higher dissolved inorganic carbon (DIC) concentrations, the higher FCO_2 rates per surface water area reported in the northern part could partly be due to an overestimation of their pCO_2 values. However, a direct comparison of average pCO_2 values does not confirm this hypothesis. For the two Maine rivers (Kennebec and Androscoggin rivers), Hunt et al. (2014) report an average pCO_2 calculated from pH and DIC of 3064 µatm. In our data set, three sampling stations are also located in these rivers and present lower median pCO_2 values of 2409, 901 and 1703 µatm for Kennebec River at Bingham and North Sidney and for Androscoggin River at Brunswick, respectively. A probable reason for the discrepancy could be that we report median values per month while Hunt et al. (2014) report arithmetic means, which are typically higher.

On the continental shelf, the shallowest depth interval is a CO_2 source in the North section while all other depth intervals are CO_2 sinks (Table 2). The magnitude of the air–sea exchange for each segment is between the values calculated for estuaries (50 gC m^{-2} yr^{-1}) and the nearby open ocean (∼20 gC m^{-2} yr^{-1}, according to Takahashi et al., 2009). This trend along a depth transect, suggesting a more pronounced continental influence on nearshore waters and a strengthening of the CO_2 shelf sink away from the coast was already discussed in the regional analysis of Chavez et al. (2007) and by Jiang et al. (2013), specifically for the South Atlantic Bight. Modeling studies over a larger domain including the upper slope of the continental shelf also suggest that the coastal waters of the Northeast US are not a more intense CO_2 sink than the neighboring open ocean (Fennel

and Wilkin, 2009; Fennel, 2010). Our analysis further suggests that the continental influence is more pronounced in the North section. Here, the shallowest waters (S1) are strong net sources of CO_2 while the intensity of the CO_2 sink for the other depth intervals gradually decreases, but only to a maximum value of $-4\,\mathrm{gC\,m^{-2}\,yr^{-1}}$ for S5. This value is about 3 times smaller than in the South section ($-12\,\mathrm{gC\,m^{-2}\,yr^{-1}}$).

Annually, river and estuarine waters of the entire COSCAT 827 outgas 3.0 ± 0.5 and $0.8 \pm 0.5\,\mathrm{TgC\,yr^{-1}}$, respectively, while continental shelf waters take up $1.7 \pm 0.3\,\mathrm{TgC\,yr^{-1}}$ (Fig. 3c). The total riverine carbon load exported from rivers to estuaries for the same area has been estimated to be $4.65\,\mathrm{TgC\,yr^{-1}}$, 45 % as dissolved and particulate organic carbon ($2.10\,\mathrm{TgC\,yr^{-1}}$, Mayorga et al., 2010) and 55 % as dissolved inorganic carbon ($2.55\,\mathrm{TgC\,yr^{-1}}$, Hartmann et al., 2009). The ratio of organic to inorganic carbon in the river loads is about 1 in the North section and 1.4 in the South section. This difference stems mainly from a combination of different lithogenic characteristics in both sections and the comparatively higher occurrence of organic soils in the North section (Hunt et al., 2013; Hossler and Bauer, 2013). Estimates of the total amount of terrestrial carbon transferred to the riverine network are not available, but the sum of the river export and the outgassing, which ignores the contribution of carbon burial and lateral exchange with wetlands, provides a lower bound estimate of $7.65\,\mathrm{TgC\,yr^{-1}}$. Under this hypothesis, ~ 40 % of the terrestrial carbon exported to rivers is emitted to the atmosphere before reaching estuaries. In spite of higher emission rates per unit surface area in the North section (Table 2), the overall efficiency of the riverine carbon filter is essentially the same in the two sections (40 and 38 % outgassing for the North and the South sections, respectively). On the shelf, however, the South section exhibits a significantly more intense CO_2 sink ($-1.25 \pm 0.2\,\mathrm{TgC\,yr^{-1}}$) than in the North section ($-0.47 \pm 0.2\,\mathrm{TgC\,yr^{-1}}$). A possible reason for this difference can be found in the contribution of the estuarine carbon filter. In the South section, where 96 % of the estuarine surface area is located, these systems contribute to an outgassing of $0.73\,\mathrm{TgC\,yr^{-1}}$ while in the North section, their influence is negligible. Cole and Caraco (2001) estimated that 28 % of the DOC entering the relatively short Hudson River estuary is respired in situ before reaching the continental shelf and it is thus likely that the estuarine outgassing in the South section is fueled by the respiration of the organic carbon loads from rivers. In contrast, the absence of estuaries in the North section favors the direct export of terrestrial organic carbon onto continental shelf waters where it can be buried and decomposed. The respiration of terrestrial organic carbon could therefore explain why the strength of the shelf CO_2 sink is weaker in this portion of the domain. Such filtering of a significant fraction of the terrestrial carbon inputs by estuaries has been evidenced in other systems (Amann et al., 2010; 2015). This view is further substantiated by the similar cumulated estuarine and continental shelf FCO_2 fluxes in both sections (Fig. 3a and b). Naturally, other environmental and physical factors also influence the carbon dynamics in shelf waters and contribute to the difference in CO_2 uptake intensity between both sections. For instance, in the North section, the Gulf of Maine is a semi-enclosed basin characterized by specific hydrological features and circulation patterns (Salisbury et al., 2008; Wang et al., 2013) which could result in longer water residence times promoting the degradation of shelf-derived organic carbon. Other potential factors include the plume of the Saint Lawrence Estuary, which has also been shown to transiently expend over the Scotian Shelf (Kang et al., 2013), the strong temperature gradient, and the heterogeneous nutrient availability along the region which may result in different phytoplankton responses (Vandemark et al., 2011; Shadwick et al., 2011). Additionally, modeling studies evidenced the potential influence of sediment denitrification on water pCO_2 through the removal of fixed nitrogen in the water column and consequent inhibition of primary production (Fennel et al., 2008; Fennel, 2010). This removal was estimated to be of similar magnitude as the lateral nitrogen loads, except for estuaries of the Mid-Atlantic Bight (MAB) region (Fennel, 2010). It can nonetheless be suggested that the estuarine carbon filter in the South section of COSCAT 827 is an important control factor of the CO_2 sink in the Mid-Atlantic Bight, which is stronger than in any other area along the entire Atlantic coast of the US (Signorini et al., 2013).

4 Conclusions

Our data-driven spatially and seasonally resolved budget analysis captures the main characteristics of the air–water CO_2 exchange along the LOAC of COSCAT 827. It evidences the contrasting dynamics of the North and South sections of the study area and an overall gradual shift from a strong source in small streams oversaturated in CO_2 towards a net sink in continental shelf waters. Our study reveals that ice and snow cover are important controlling factors of the seasonal dynamics of CO_2 outgassing in streams and rivers and account for a large part of the difference between the North and South sections. The close simultaneity of the snowmelt on land and of the phytoplankton bloom on the continental shelf leads to opposite temporal dynamics in FCO_2 in these two compartments of the LOAC. In addition, our results reveal that estuaries filter significant amounts of terrestrial carbon inputs, thereby influencing the continental shelf carbon uptake. Although this process likely operates in conjunction with other regional physical processes, it is proposed that the much stronger estuarine carbon filter in the South section contributes to a strengthening of the CO_2 sink in the adjacent continental shelf waters.

Acknowledgements. The research leading to these results received funding from the European Union's Seventh Framework Program (FP7/2007-2013) under grant agreement no. 283080, project GEOCARBON. G. G. Laruelle is Chargé de recherches du F.R.S.-FNRS at the Université Libre de Bruxelles. Ronny Lauerwald was funded by the French Agence Nationale de la Recherche (Investissement d'Avenir no. ANR-10-LABX-0018). Jens Hartmann was funded by DFG-project EXC 177. The Surface Ocean CO_2 Atlas (SOCAT) is an international effort, supported by the International Ocean Carbon Coordination Project (IOCCP), the Surface Ocean Lower Atmosphere Study (SOLAS), and the Integrated Marine Biogeochemistry and Ecosystem Research program (IMBER), in order to deliver a uniformly quality-controlled surface ocean CO_2 database. The many researchers and funding agencies responsible for the collection of data and quality control are thanked for their contributions to SOCAT. This work also used data extracted from the SOCAT/MARCATS segmentation (Laruelle et al., 2013), the CCMP wind database (Atlas et al., 2010), GLOBALNEWS2 (Mayorga et al., 2010; Hartmann et al., 2009), the SRTM water body data set (NASA/NGA, 2003), HydroSHEDS 15 s routing scheme, the average annual runoff data extracted from the UNH/GRDC composites (Fekete et al., 2002), the global lake and wetland database of Lehner and Döll (2004), and mean air temperature derived from the WorldClim data set of Hijmans et al. (2005).

Edited by: K. Fennel

References

Amann, T., Weiss, A., and Hartmann, J.: Inorganic carbon fluxes in the inner Elbe estuary, Germany, Estuar. Coasts, 38, 192–210, 2015.

Amann, T., Weiss, A., and Hartmann, J.: Carbon dynamics in the freshwater part of the Elbe estuary, Germany, Estuar. Coast. Shelf S., 107, 112–121, 2012.

Aufdenkampe, A. K., Mayorga, E., Raymond, P. A., Melack, J. M., Doney, S. C., Alin, S. R., Aalto, R. E., and Yoo, K.: Riverine coupling of biogeochemical cycles between land, oceans, and atmosphere, Front. Ecol. Environ., 9, 53–60, doi:10.1890/100014, 2011.

Armstrong, R. L. and Brodzik, M. J.: Recent Northern Hemisphere snow extent: A comparison of data derived from visible and microwave satellite sensors, Geophys. Res. Lett., 28, 3673–3676, 2001.

Atlas, R., Hoffman, R. N., Ardizzone, J., Leidner, S. M., Jusem, J. C., Smith, D. K., and Gombos, D.: A cross-calibrated, multiplatform ocean surface wind velocity product for meteorological and oceanographic applications, Bull. Am. Meteor. Soc., 92, 157–174, doi:10.1175/2010BAMS2946.1, 2011.

Bakker, D. C. E., Pfeil, B., Smith, K., Hankin, S., Olsen, A., Alin, S. R., Cosca, C., Harasawa, S., Kozyr, A., Nojiri, Y., O'Brien, K. M., Schuster, U., Telszewski, M., Tilbrook, B., Wada, C., Akl, J., Barbero, L., Bates, N. R., Boutin, J., Bozec, Y., Cai, W.-J., Castle, R. D., Chavez, F. P., Chen, L., Chierici, M., Currie, K., de Baar, H. J. W., Evans, W., Feely, R. A., Fransson, A., Gao, Z., Hales, B., Hardman-Mountford, N. J., Hoppema, M., Huang, W.-J., Hunt, C. W., Huss, B., Ichikawa, T., Johannessen, T., Jones, E. M., Jones, S. D., Jutterström, S., Kitidis, V., Körtzinger, A., Landschützer, P., Lauvset, S. K., Lefèvre, N., Manke, A. B., Mathis, J. T., Merlivat, L., Metzl, N., Murata, A., Newberger, T., Omar, A. M., Ono, T., Park, G.-H., Paterson, K., Pierrot, D., Ríos, A. F., Sabine, C. L., Saito, S., Salisbury, J., Sarma, V. V. S. S., Schlitzer, R., Sieger, R., Skjelvan, I., Steinhoff, T., Sullivan, K. F., Sun, H., Sutton, A. J., Suzuki, T., Sweeney, C., Takahashi, T., Tjiputra, J., Tsurushima, N., van Heuven, S. M. A. C., Vandemark, D., Vlahos, P., Wallace, D. W. R., Wanninkhof, R., and Watson, A. J.: An update to the Surface Ocean CO_2 Atlas (SOCAT version 2), Earth Syst. Sci. Data, 6, 69–90, doi:10.5194/essd-6-69-2014, 2014.

Battin, T. J., Luyssaert, S., and Kaplan, L. A.: The boundless carbon cycle, Nat. Biogeosci., 2, 598–600, 2009.

Bauer, J. E., Cai, W.-J., Raymond, P. A., Bianchi, T. S., Hopkinson, C. S., and Regnier, P. A. G.: The changing carbon cycle of the coastal ocean, Nature, 504, 61–70, doi:10.1038/nature12857, 2013.

Borges, A. V., Delille, B., and Frankignoulle, M.: Budgeting sinks and sources of CO_2 in the coastal ocean: diversity of ecosystems counts, Geophys. Res. Lett. 32, L14601, doi:10.1029/2005GL023053, 2005.

Butman, D. and Raymond, P. A.: Significant efflux of carbon dioxide from streams and rivers in the United States, Nat. Geosci., 4, 839–842, 2011.

Cai, W. J.: Estuarine and coastal ocean carbon paradox: CO_2 sinks or sites of terrestrial carbon incineration?, Annu. Rev. Mar. Sci., 3, 123–145, 2011.

Ciais, P., Sabine, C., Bala, G., Bopp, L., Brovkin, V., Canadell, J., Chhabra, A., De Fries, R., Galloway, J., Heimann, M., Jones, C., Le Quéré, C., Myneni, R., Piao, S., Thornton, P., Ahlström, A., Anav, A., Andrews, O., Archer, D., Arora, V., Bonan, G., Borges, A. V., Bousquet, P., Bouwman, L., Bruhwiler, L. M., Caldeira, K., Cao, L., Chappellaz, J., Chevallier, F., Cleveland, C., Cox, P., Dentener, F. J., Doney, S. C., Erisman, J. W., Euskirchen, E. S., Friedlingstein, P., Gruber, N., Gurney, K., Hopwood, B., Houghton, R. A., House, J. I., Houweling, S., Hunter, S., Hurtt, G., Jacobson, A. D., Jain, A., Joos, F., Jungclaus, J., Kaplan, J. O., Kato, E., Keeling, R., Khatiwala, S., Kirschke, S., Goldewijk, K. K., Kloster, S., Koven, C., Kroeze, C., Lamarque, J.-F., Lassey, K., Law, R. M., Lenton, A., Lomas, M. R., Luo, Y., Maki, T., Marland, G., Matthews, H. D., Mayorga, E., Melton, J. R., Metzl, N., Munhoven, G., Niwa, Y., Norby, R. J., O'Connor, F., Orr, J., Park, G.-H., Patra, P., Peregon, A., Peters, W., Peylin, P., Piper, S., Pongratz, J., Poulter, B., Raymond, P. A., Rayner, P., Ridgwell, A., Ringeval, B., Rödenbeck, C., Saunois, M., Schmittner, A., Schuur, E., Sitch, S., Spahni, R., Stocker, B., Takahashi, T., Thompson, R. L., Tjiputra, J., van der Werf, G., van Vuuren, D., Voulgarakis, A., Wania, R., Zaehle, S. and Zeng, N.: Chapter 6: Carbon and Other Biogeochemical Cycles, in: Climate Change 2013 The Physical Science Basis, editd by: Stocker, T., Qin D., and Platner G.-K., Cambridge University Press, Cambridge, 2013.

Chavez, F. P., Takahashi, T., Cai, W.-J., Friederich, G., Hales, B., Wanninkhof, R., and Feely, R.: Coastal oceans. The First State of the Carbon Cycle Report (SOCCR): The North American Carbon Budget and Implications for the Global Carbon Cycle, edited by: King A. W., Dilling L., Zimmerman G. P., Fairman D. M., Houghton R. A., Marland G., Rose A. Z., Wilbanks T. J., NOAA, Maryland, USA, 157–166, 2007.

Chen, C.-T. A., Huang, T.-H., Chen, Y.-C., Bai, Y., He, X., and Kang, Y.: Air-sea exchanges of CO_2 in the world's coastal seas, Biogeosciences, 10, 6509–6544, doi:10.5194/bg-10-6509-2013, 2013.

Cole, J. J. and Caraco, N. F.: Carbon in catchments: Connecting terrestrial carbon losses with aquatic metabolism, Mar. Freshwater Res., 52, 101–110, doi:10.1071/MF00084, 2001.

Cole, J. J., Prairie, Y. T., Caraco, N. F., McDowell, W. H., Tranvik, L. J., Striegl, R. G., Duarte, C. M., Kortelainen, P., Downing, J. A., Middelburg, J. J., and Melack, J.: Plumbing the global carbon cycle: Integrating inland waters into the terrestrial carbon budget, Ecosystems, 10, 171–184, 2007.

Dai, M., Cao, Z., Guo, X., Zhai, W., Liu, Z., Yin, Z., Xu, Y., Gan, J., Hu, J., and Du, C.: Why are some marginal seas sources of atmospheric CO_2?, Geophys. Res. Lett., 40, 2154–2158, 2013.

Degrandpré, M. D., Olbu, G. J., Beatty, M., and Hammar, T. R.: Air-sea CO_2 fluxes on the US Middle Atlantic Bight, Deep-Sea Res. II, 49, 4355–4367, 2002.

Fekete, B. M., Vorosmarty, C. J., Grabs, W., and Vörösmarty, C. J.: High-resolution fields of global runoff combining observed river discharge and simulated water balances, Global Biogeochem. Cy., 16, 15-1–15-10 doi:10.1029/1999gb001254, 2002.

Fennel, K.: The role of continental shelves in nitrogen and carbon cycling: Northwestern North Atlantic case study, Ocean Sci., 6, 539–548, doi:10.5194/os-6-539-2010, 2010.

Fennel, K. and Wilkin, J.: Quantifying biological carbon export for the northwest North Atlantic continental shelves, Geophys. Res. Lett., 36, L18605, doi:10.1029/2009GL039818, 2009.

Fennel, K., Wilkin, J., Previdi, M., and Najjar, R.: Denitrification effects on air-sea CO_2 flux in the coastal ocean: Simulations for the Northwest North Atlantic, Geophys. Res. Lett., 35, L24608, doi:10.1029/2008GL036147, 2008.

Frankignoulle, M., Abril, G., Borges, A., Bourge, I., Canon, C., Delille, B., Libert, E., and Théate, J.-M.: Carbon dioxide emission from European estuaries, Science, 282, 434–436, doi:10.1126/science.282.5388.434, 1998.

Finlay, C. F.: Controls of streamwater dissolved inorganic carbon dynamics in a forested watershed, Biogeochem., 62, 231–252, 2003.

Hartmann, J., Jansen, N., Dürr, H. H., Kempe, S., and Köhler, P.: Global CO_2-consumption by chemical weathering: What is the contribution of highly active weathering regions?, Global Planet. Change, 69, 185–194, doi:10.1016/j.gloplacha.2009.07.007, 2009.

Hartmann, J., Lauerwald, R., and Moosdorf, N.: A brief overview of the GLObal RIver CHemistry Database, GLORICH, Procedia, Earth Planet. Sci., 10, 23–27, 2014.

Henry, W.: Experiments on the Quantity of Gases Absorbed by Water, at Different Temperatures, and under Different Pressures, Philos. T. R. Soc., 93, 29–274, doi:10.1098/rstl.1803.0004, 1803.

Hijmans, R. J., Cameron, S. E., Parra, J. L., Jones, P. G., and Jarvis, A.: Very high resolution interpolated climate surfaces for global land areas, Int.l J. Climatol., 25, 1965–1978, doi:10.1002/joc.1276, 2005.

Hossler, K. and Bauer, J. E.: Amounts, isotopic character, and ages of organic and inorganic carbon exported from rivers to ocean margins: 1. Estimates of terrestrial losses and inputs to the Middle Atlantic Bight, Global Biogeochem. Cy., 27, 331–346, doi:10.1002/gbc.20033, 2013

Hunt, C. W., Salisbury, J. E., Vandemark, D., and McGillis, W.: Contrasting Carbon Dioxide Inputs and Exchange in Three Adjacent New England Estuaries. Estuar. Coast., 34, 68–77, doi:10.1007/s12237-010-9299-9, 2010.

Hunt, C. W., Salisbury, J. E., and Vandemark, D.: Contribution of non-carbonate anions to total alkalinity and overestimation of pCO_2 in New England and New Brunswick rivers, Biogeosciences, 8, 3069–3076, doi:10.5194/bg-8-3069-2011, 2011.

Hunt, C. W., Salisbury, J. E., and Vandemark, D.: CO_2 Input Dynamics and Air-Sea Exchange in a Large New England Estuary, Estuar. Coast., 37, 1078–1091, 2014.

Jiang, L.-Q., Cai, W.-J., Wang, Y., and Bauer, J. E.: Influence of terrestrial inputs on continental shelf carbon dioxide, Biogeosciences, 10, 839–849, doi:10.5194/bg-10-839-2013, 2013.

Jones, J. B. and Mulholland, P. J.: Carbon dioxide variation in a hardwood forest stream: An integrative measure of whole catchment soil respiration, Ecosystems, 1, 183–196, 1998.

Kang, Y., Pan, D., Bai, Y., He, X., Chen, X., Chen, C.-T. A., and Wang, D.: Areas of the global major river plumes, Acta. Oceanol. Sin., 32, 79–88, doi:10.1007/s13131-013-0269-5, 2013.

Kempe, S.: Long-term records of CO_2, pressure fluctuations in fresh waters, Mitt. Geol.-Palaeontol. Inst. Univ. Hamburg 52, 9, l–332, 1982.

Laruelle, G. G., Dürr, H. H., Slomp, C. P., and Borges, A. V.: Evaluation of sinks and sources of CO_2 in the global coastal ocean using a spatially-explicit typology of estuaries and continental shelves, Geophys. Res. Lett., 37, L15607, doi:10.1029/2010GL043691, 2010.

Laruelle, G. G., Dürr, H. H., Lauerwald, R., Hartmann, J., Slomp, C. P., Goossens, N., and Regnier, P. A. G.: Global multi-scale segmentation of continental and coastal waters from the watersheds to the continental margins, Hydrol. Earth Syst. Sci., 17, 2029–2051, doi:10.5194/hess-17-2029-2013, 2013.

Laruelle, G. G., Lauerwald, R., Pfeil, B., and Regnier, P.: Regionalized global budget of the CO_2 exchange at the air-water interface in continental shelf seas, Global Biogeochem. Cy., 28, 1199–1214, doi:10.1002/2014GB004832, 2014.

Lauerwald, R., Hartmann, J., Moosdorf, N., Kempe, S., and Raymond, P. A.: What controls the spatial patterns of the riverine carbonate system? – A case study for North America, Chemical Geology, 337, 114–127, 2013.

Lauerwald, R., Laruelle, G. G., Hartmann, J., Ciais, P., Regnier, P. A. G.: Spatial patterns in CO_2 evasion from the global river network Global Biogeochem. Cy., in review, 2015.

Lehner, B. and Döll, P.: Development and validation of a global database of lakes, reservoirs and wetlands, J. Hydrol., 296, 1–22, doi:10.1016/j.jhydrol.2004.03.028, 2004.

Lehner, B., Verdin, K., and Jarvis, A.: New global hydrography derived from spaceborne elevation data, Eos, Transactions, AGU, 89, 93–94, 2008.

Mackenzie, F. T., De Carlo, E. H., and Lerman, A.: Coupled C, N, P, and O Biogeochemical Cycling at the Land-Ocean Interface, in: Treatise on Estuarine and Coastal Science, edited by: Middelburg J. J., Laane R., Elsevier, the Netherlands, 2012.

Mayorga, E., Seitzinger, S. P., Harrison, J. A., Dumont, E., Beusen, A. H. W., Bouwman, A. F., Fekete, B. M., Kroeze, C., and Van Drecht, G.: Global Nutrient Export from WaterSheds 2 (NEWS2): Model development and implementation, Environ.

Model. Softw., 25, 837–853, doi:10.1016/j.envsoft.2010.01.007, 2010.

Meybeck, M., Dürr, H. H., and Vörosmarty, C. J.: Global coastal segmentation and its river catchment contributors: A new look at land-ocean linkage, Global Biogeochem. Cy., 20, GB1S90, doi:10.1029/2005GB002540, 2006.

NASA/NGA: SRTM Water Body Data Product Specific Guidance, Version 2.0, 2003.

Parkhurst, D. L. and Appelo, C. A. J.: User's guide to PHREEQC (version 2) – a computer program for speciation, reaction-path, 1D-transport, and inverse geochemical calculations, US Geol. Surv. Water Resour. Inv. Rep., 99–4259, 1999.

Previdi, M., Fennel, K., Wilkin, J., and Haidvogel, D. B.: Interannual Variability in Atmospheric CO_2 Uptake on the Northeast U.S. Continental Shelf, J. Geophys. Res., 114, G04003, doi:10.1029/2008JG000881, 2009.

Raymond, P. A. and Hopkinson, C. S.: Ecosystem Modulation of Dissolved Carbon Age in a Temperate Marsh-Dominated Estuary, Ecosystems, 6, 694–705, 2003.

Raymond, P. A., Caraco, N. F., and Cole, J. J.: Carbon Dioxide Concentration and Atmospheric Flux in the Hudson River, Estuaries, 20, 381–390, 1997.

Raymond, P. A., Bauer, J. E., and Cole, J. J.: Atmospheric CO_2 evasion, dissolved inorganic carbon production, and net heterotrophy in the York River estuary, Limnol. Oceanogr., 45, 1707–1717, 2000.

Raymond, P. A., Zappa, C. J., Butman, D., Bott, T. L., Potter, J., Mulholland, P., Laursen, A. E., McDowell, W. H., and Newbold, D.: Scaling the gas transfer velocity and hydraulic geometry in streams and small rivers, Limnol. Oceanogr., 2, 41–53, doi:10.1215/21573689-1597669, 2012.

Raymond, P. A., Hartmann, J., Lauerwald, R., Sobek, S., McDonald, C., Hoover, M., Butman, D., Striegl, R., Mayorga, E., Humborg, C., Kortelainen, P., Dürr, H., Meybeck, M., Ciais, P., and Guth, P.: Global carbon dioxide emissions from inland waters, Nature, 503, 355–359, doi:10.1038/nature12760, 2013.

Rawlins, B. G., Palumbo-Roe, B., Gooddy, D. C., Worrall, F., and Smith, H.: A model of potential carbon dioxide efflux from surface water across England and Wales using headwater stream survey data and landscape predictors, Biogeosciences, 11, 1911–1925, doi:10.5194/bg-11-1911-2014, 2014.

Regnier, P., Friedlingstein, P., Ciais, P., Mackenzie, F. T., Gruber, N., Janssens, I., Laruelle, G. G., Lauerwald, R., Luyssaert, S., Andersson, A. J., Arndt, S., Arnosti, C., Borges, A. V., Dale, A. W., Gallego-Sala, A., Goddéris, Y., Goossens, N., Hartmann, J., Heinze, C., Ilyina, T., Joos, F., LaRowe, D. E., Leifeld, J., Meysman, F. J. R., Munhoven, G., Raymond, P. A., Spahni, R., Suntharalingam, P., and Thullner, M.: Anthropogenic perturbation of the carbon fluxes from land to ocean, Nat. Geosci., 6, 597–607, doi:10.1038/ngeo1830, 2013a.

Regnier, P., Arndt, S., Goossens, N., Volta, C., Laruelle, G. G., Lauerwald, R. and Hartmann, J.: Modeling estuarine biogeochemical dynamics: from the local to the global scale. Aquat. Geochem., 19, 591–626, 2013b.

Salisbury, J. E., Vandemark, D., Hunt, C. W., Campbell, J. W., McGillis, W. R., and McDowell, W. H.: Seasonal observations of surface waters in two Gulf of Maine estuary-plume systems: Relationships between watershed attributes, optical measurements and surface pCO_2, Estuarine Coastal Shelf Sci., 77, 245–252, 2008.

Shadwick, E. H., Thomas, H., Comeau, A., Craig, S. E., Hunt, C. W., and Salisbury, J. E.: Air-Sea CO_2 fluxes on the Scotian Shelf: seasonal to multi-annual variability, Biogeosciences, 7, 3851–3867, doi:10.5194/bg-7-3851-2010, 2010.

Shadwick, E. H., Thomas, H., Azetsu-Scott, K., Greenan, B. J. W., Head, E., and Horne, E.: Seasonal variability of dissolved inorganic carbon and surface water pCO_2 in the Scotian Shelf region of the Northwestern, Atlantic, Mar. Chem., 124, 23–37, 2011.

Signorini, S. R., Mannino, A., Najjar Jr., R. G., Friedrichs, M. A. M., Cai, W.-J., Salisbury, J., Wang, Z. A., Thomas, H., and Shadwick, E.: Surface ocean pCO_2 seasonality and sea-air CO_2 flux estimates for the North American east coast, J. Geophys. Res.-Oceans, 118, 5439–5460, doi:10.1002/jgrc.20369, 2013.

Strahler, A. N.: Hypsometric (area-altitude) analysis of erosional topology, Geol. Soc. Am. Bull., 63, 1117–1142, doi:10.1130/0016-7606(1952)63[1117:HAAOET]2.0.CO;2, 1952.

Striegl, R. G., Dornblaser, M. M., McDonald, C. P., Rover, J. R., and Stets, E. G.: Carbon dioxide and methane emissions from the Yukon River system, Global Biogeochem. Cy., 26, GB0E05 , 2012.

Takahashi, T., Sutherland, S. C., Wanninkhof, R., Sweeney, C., Feely, R. A., Chipman, D. W., Hales, B., Friederich, G., Chavez, F., Sabine, C., Watson, A., Bakker, D. C. E., Schuster, U., Metzl, N., Yoshikawa-Inoue, H., Ishii, M., Midorikawa, T., Nojiri, Y., Körtzinger, A., Steinhoff, T., Hoppema, M., Olafsson, J., Arnarson, T. S., Tilbrook, B., Johannessen, T., Olsen, A., Bellerby, R., Wong, C. S., Delille, B., Bates, N. R., and de Baar, H. J. W.: Climatological mean and decadal change in surface ocean pCO_2, and net sea-air CO_2 flux over the global oceans, Deep-Sea Res. II, 56, 554–577, 2009.

Telmer, K. and Veizer, J.: Carbon fluxes, pCO_2 and substrate weathering in a large northern river basin, Canada: Carbon isotope perspectives, Chem. Geol., 151, 61–86, 1999.

Teodoru, C. R., del Giorgio, P. A., Prairie, Y. T., and Camire, M.: Patterns in pCO_2 in boreal streams and rivers of northern Quebec, Canada, Global Biogeochem. Cy., 23, GB2012, doi:10.1029/2008GB003404, 2009.

Thomas, H. and Schneider, B.: The seasonal cycle of carbon dioxide in Baltic Sea surface waters, J. Mar. Syst., 22, 53–67, doi:10.1016/s0924-7963(99)00030-5, 1999.

Vandemark, D, Salisbury, J. E, Hunt, C. W, Shellito, S. M, Irish, J. D, McGillis,W. R, Sabine, C. L, and Maenner, S. M.: Temporal and spatial dynamics of CO_2 air-sea flux in the Gulf of Maine, J. Geophys. Res.-Oceans, 116, C01012, doi:10.1029/2010JC006408, 2011.

Wallin, M. B., Oquist, M. G., Buffam, I., Billett, M. F., Nisell, J., Bishop, K. H., and Öquist, M. G.: Spatiotemporal variability of the gas transfer coefficient (K-CO_2) in boreal streams: Implications for large scale estimates of CO_2 evasion, Global Biogeochem. Cy., 25, GB3025, doi:10.1029/2010gb003975, 2011.

Wang, Z. A., Wanninkhof, R., Cai, W.-J., Byrne, R. H., Hu, X., Peng, T. H., and Huang, W. J.: The marine inorganic carbon system along the Gulf of Mexico and Atlantic Coasts of the United States: Insights from a transregional coastal carbon study, Limnol. Oceanogr., 58, 325–342, 2013.

Wanninkhof, R.: Relationship between wind speed and gas exchange over the ocean, J. Geophys. Res., 97, 7373–7382, 1992.

Wanninkhof, R., Park, G.-H., Takahashi, T., Sweeney, C., Feely, R., Nojiri, Y., Gruber, N., Doney, S. C., McKinley, G. A., Lenton, A., Le Quéré, C., Heinze, C., Schwinger, J., Graven, H., and Khatiwala, S.: Global ocean carbon uptake: magnitude, variability and trends, Biogeosciences, 10, 1983–2000, doi:10.5194/bg-10-1983-2013, 2013.